NACA

RESEARCH MEMORANDUM

TESTS OF AERODYNAMICALLY HEATED MULTIWEB WING

STRUCTURES IN A FREE JET AT MACH NUMBER 2

TWO ALUMINUM-ALLOY MODELS OF 20-INCH CHORD

WITH 0.064-INCH-THICK SKIN AT ANGLES

OF ATTACK OF 0° AND ±2°

By Georgene H. Miltonberger, George E. Griffith,
and John R. Davidson

Langley Aeronautical Laboratory
Langley Field, Va.

NATIONAL ADVISORY COMMITTEE
FOR AERONAUTICS

WASHINGTON

October 28, 1957

NACA RM L57H19 CONFIDENTIAL

NATIONAL ADVISORY COMMITTEE FOR AERONAUTICS

RESEARCH MEMORANDUM

TESTS OF AERODYNAMICALLY HEATED MULTIWEB WING

STRUCTURES IN A FREE JET AT MACH NUMBER 2

TWO ALUMINUM-ALLOY MODELS OF 20-INCH CHORD

WITH 0.064-INCH-THICK SKIN AT ANGLES

OF ATTACK OF 0° AND ±2°

By Georgene H. Miltonberger, George E. Griffith,
and John R. Davidson

SUMMARY

Two identically constructed 2024-T3 aluminum-alloy multiweb-wing structures, models MW-2-(2) and MW-2-(3), were tested under aerodynamic conditions similar to those encountered in supersonic flight at a Mach number of 2. Model MW-2-(2) was tested four times at an angle of attack of 0° and once at an angle of attack of -2° before experiencing a static-type failure at an angle of attack of 2°. Model MW-2-(3) was tested at angles of attack of 0° and -2° and survived both tests with no visible damage. The models were instrumented to obtain temperatures, pressures, and strains. In general, temperature and pressure data were in good agreement with calculated values; strain data were used only to provide frequency and phasing information and to help reconstruct model behavior. High-speed motion pictures provided a pictorial record of the model behavior.

INTRODUCTION

As part of an investigation of the effects of aerodynamic heating on aircraft structures, the Structures Research Division of the Langley Laboratory is testing multiweb wings under aerodynamic conditions similar to those encountered in supersonic flight. The first multiweb wing, model MW-1, experienced a dynamic failure; details of the test results and failure are presented in reference 1. The second multiweb wing,

CONFIDENTIAL

model MW-2, was essentially a $\frac{1}{2}$-scale version of model MW-1, and the
third multiweb wing, model MW-3, other than having a thicker skin, was
similar to model MW-2. Model MW-2 experienced a partial dynamic failure
at an angle of attack of 0°, whereas model MW-3 failed statically at an
angle of attack of 5° after surviving four tests at smaller angles of
attack; the results of the tests on these two models are discussed in
detail in reference 2.

Test results of four additional multiweb wing structures are pre-
sented in reference 3. Each of these models varied from model MW-2 by
either a reduction in tip-bulkhead thickness, the inclusion of ribs, the
inclusion of ribs combined with a reduction in skin thickness, or a change
in material. Of these four models only the one with the reduced tip-
bulkhead thickness failed. Thus, the results of the tests on the first
seven models indicate that minor structural modifications to model MW-2
can either prevent or precipitate failure when tested at Mach 2 sea-level
conditions and, therefore, that model MW-2 is a marginal wing structure
under these test conditions.

In order to obtain additional information on the behavior of the
MW-2-type structure and on the failure of the original model, duplicate
models were built and tested. The present paper discusses in detail the
test results of two such duplicates, models MW-2-(2) and MW-2-(3). Six
tests were made on model MW-2-(2): four tests at an angle of attack
of 0°, one at -2°, and one at 2°. Two tests were made on model MW-2-(3):
one at an angle of attack of 0° and one at -2°.

SYMBOLS

c_p specific heat of air, Btu/(slug)(°F)

C_p pressure coefficient, $\dfrac{p_m - p_\infty}{q_\infty}$

h heat-transfer coefficient, Btu/(sq ft)(sec)(°F), except as
             noted

x distance along model chord from leading edge, ft

N_{St} Stanton number, $h/c_p \rho V$

p pressure, lb/sq in. abs

q dynamic pressure, lb/sq in.

R   Reynolds number, $\rho V l/\mu$

t   time from start of air flow, sec

T   temperature, $^\circ$F

V   velocity of air, ft/sec

μ absolute viscosity of air, slugs/(ft)(sec)

ρ density of air, slugs/cu ft

Subscripts:

aw   adiabatic wall

j   joint conditions

m   model

o   initial conditions

t   tunnel stagnation conditions

∞ free-stream conditions

APPARATUS AND TESTS

Models

The models designated MW-2-(2) and MW-2-(3) were duplicates of model MW-2 (ref. 2); they represented somewhat idealized semispan multiweb wings with 5-percent-thick, symmetrical, circular-arc airfoil sections. All material was 2024-T3 (24S-T3) aluminum alloy except that the rivets were either 2117-T(17S-T) aluminum-alloy rivets or Huck rivets; steel screws were used to attach the skins to the tip bulkhead. Each model was canti-levered from its root bulkhead; the portion of the model containing the root bulkhead was clamped between steel angles which were in turn attached to the test stand. Pertinent dimensions and details of construction of the models are given in figure 1. The surfaces of the models were painted with zinc chromate, and a grid of black lacquer was then added to assist in viewing the high-speed motion pictures of the model behavior during the tests.

As a result of inaccuracies in fabrication, model MW-2-(2) had approximately 0.21° "built-in" twist from tip to root and model MW-2-(3) had approximately 0.08° built-in twist from tip to root.

Instrumentation

Both models were instrumented with iron-constantan thermocouples and SR-4 type EBDF-7D temperature-compensated (50° F to 250° F) wire strain gages. The instrumentation on model MW-2-(2) consisted of 30 thermocouples and 19 strain gages, as shown in figure 2. The majority of the wire strain gages were located near the tip of the model to obtain data on the phasing and frequency of model vibrations. The instrumentation on model MW-2-(3) consisted of 12 thermocouples, 7 strain gages, and 59 pressure orifices, as shown in figures 3 and 4. Ten differential pressures and 39 pressures were measured by using three types of pressure-sensing instruments: miniature differential pressure pickups, pressure transducers, and six-capsule manometers. The miniature gages (those having the highest frequency response) were located in the region near the tip to obtain information on the frequency of model vibrations.

Supplementary data were obtained from 16-millimeter motion-picture cameras. For each test, motion-picture cameras operating at approximate speeds of either 600, 1,000, or 1,600 frames per second were used to record the behavior of the model.

The estimated probable errors in the individual measurements of the tabulated data are as follows:

Stagnation pressure, lb/sq in. . . . . ±0.7
Stagnation temperature, °F . . . . ±3
Model temperature, °F . . . . ±3

Calibration tests showed the Mach number to be 1.99 ± 0.02.

Natural Modes and Frequencies

Prior to the aerodynamic tests, models MW-2-(2) and MW-2-(3) were vibrated at room temperature to determine their natural modes and frequencies. A comparison of the dynamic characteristics of these two copies with those of the original model MW-2 is desirable, since the behavior of the copies during the aerodynamic tests differed markedly from that of the original structure. Although the modes and frequencies of the original model MW-2 had not been determined, modes and frequencies of two additional copies of the MW-2 type (models MW-2-(4) and MW-2-(5)) were obtained and are compared with those of models MW-2-(2) and MW-2-(3) in table I.

Two values of frequency are given for model MW-2-(2); the first value is that obtained before any aerodynamic tests and the second is that obtained after the first two aerodynamic tests (a cold and a hot test at an angle of attack of 0°). Although model MW-2-(2) survived these two tests with no visible damage, the lower frequencies obtained indicate that this type of aerodynamic testing has a tendency to reduce the stiffness of the structure or to weaken the model.

The pressure gages and attendant tubing inside model MW-2-(3) (fig. 4) undoubtedly had some effect on the modes and frequencies of this model. The additional mass of the miniature gages and mounting assemblies located near the tip of the model tends to lower the modal frequencies; on the other hand, the considerable amount of tubing leading from the pressure gages and the orifices to the root of the model contributes a stiffening effect. The combined effects are probably manifested in lower frequencies and in changes in modes. (Note, for example, that mode E is similar to mode D.) The net result on the stiffness of model MW-2-(3) of the addition of the gages and tubing cannot be predicted with certainty, but the fact that this model apparently experienced fewer modes in the frequency range shown in table I indicates some overall stiffening effect.

In general, however, the results shown in table I imply no drastic changes in stiffness from model to model. It should be kept in mind that these results were obtained without heating and without the presence of thermal stress, such as would be encountered in the aerodynamic tests.

Description of Tests

The aerodynamic tests were made at the Langley Pilotless Aircraft Research Station at Wallops Island, Va., in the preflight jet, a blow-down wind tunnel in which models are tested in a free jet at the exit of a supersonic nozzle. Additional information on the characteristics of the preflight jet can be found in the appendix of reference 2. Each model was mounted vertically in the jet (root downward) with its leading edge 2 inches downstream of the nozzle-exit plane. During each test a flat plate or fence surrounded the model approximately $19\frac{7}{8}$ inches below the model tip so that the fence projected 1/8 inch above the lower jet boundary and shielded the supporting structure from the airstream. (See fig. 5.)

Eight tests were made on the two models at a Mach number of 1.99. All were hot tests, 474° F $\leq T_t \leq 540^\circ$ F, except for one cold test, $T_t = 89^\circ$ F. The stagnation temperatures approached test values within 1 second after the beginning of air flow. For all hot runs, the stagnation pressure of approximately 115 lb/sq in. abs was attained in

2 seconds or less after the start of air flow from the nozzle and then fluctuated about this value until approximately 11 seconds. However, for the cold run the stagnation pressure attained was approximately 101 lb/sq in. abs. Test time was reckoned from the time air began to flow out of the nozzle, and test conditions were considered to exist whenever the stagnation pressure equaled or exceeded 100 lb/sq in. abs, except that for the last test on model MW-2-(2) when failure occurred, test conditions ended at the time of failure. Detailed test conditions are given in table II.

Six tests were made on model MW-2-(2), four at an angle of attack of 0°, one at -2°, and one at 2°; two tests were made on model MW-2-(3), one at an angle of attack of 0° and one at -2°. The angle of attack was obtained by rotating the model about a point $1\frac{1}{2}$ inches downstream of the trailing edge – a clockwise rotation of the model, when viewed from the tip, indicates positive angle of attack. In both models the built-in twist was in the direction of positive angle of attack; consequently, for model MW-2-(2) the air loads were greater at an angle of attack of 2° than at -2°. The assigned angle of attack for each of the eight tests on the two models is presented in table II. Pressures were not measured on model MW-2-(2) and, consequently, angles of attack could not be computed. However, on the two tests of model MW-2-(3) a check was made on the angle of attack by using the experimental pressure in conjunction with the calculated pressures determined for various angles of attack. Calculated pressures were obtained by using the slope found from measured model ordinates and by using second-order, small-perturbation theory; the pressures in the region affected by the model tip were modified in accord with the method of reference 4. The arithmetic average of the computed angle of attack for run 1 was -0.1° and for run 2 was -2.1° as compared with assigned values of 0° and -2°, respectively.

Tunnel Stagnation Pressure and Temperature

Stagnation pressure.- A typical variation of stagnation pressure with time is shown in figure 6(a). The values reported in table II are average stagnation pressures during test conditions ($p_t \geqq 100$ lb/sq in. abs) except that for run 6 on model MW-2-(2) the stagnation pressure is an average from the beginning of test conditions until failure.

Stagnation temperature.- A typical variation of stagnation temperature with time is shown in figure 6(b). Except for runs 5 and 6 on model MW-2-(2) (the last two tests made in the group of eight tests on the two models), the stagnation temperatures reported in table II were obtained by integrating, during the time of test conditions, the average temperature of the probes located just downstream of the model (fig. 5). However, pressure measurements on model MW-2-(3) indicated that the bow

waves formed by the two probes interfered with the shock waves at the trailing edge of the model and affected the pressure distribution; hence, the probes were removed from the fence after the tests on model MW-2-(3) but before runs 5 and 6 on model MW-2-(2). Since probe temperatures were not available for these two runs, the stagnation temperatures reported were obtained by integrating the arithmetic average temperature of selected thermocouples located upstream of the nozzle during the period of test conditions for run 5, and from the beginning of test conditions until failure for run 6. Data from model and survey tests indicated that averages from these selected thermocouples are in fair agreement with averages from the probe thermocouples.

RESULTS AND DISCUSSION

Model Temperatures

During the cold run, run 1 of model MW-2-(2), all model temperatures decreased, some as much as 22° F, from the initial temperature. These temperature decreases were expected since the initial temperature was approximately that of the stagnation temperature, 89° F, and the adiabatic-wall temperature was approximately 30° F lower.

Test temperatures for the hot runs on models MW-2(2) and MW-2-(3) are given in tables III and IV, respectively. Plotted in figure 7 are some temperature histories for run 3 of model MW-2-(2) that are typical of the measured temperatures for both models except that the only interior temperature obtained in model MW-2-(3) (thermocouple 3) appears to be somewhat low; this lower temperature could be the result of poor joint thermal conductivity. The results shown in figure 7 illustrate the effects of heat conduction from the skin to the interior structure of the model. The tests were of insufficient length to produce steady-state temperature conditions.

Test data show that skin temperatures decreased across the model chordwise from leading edge to trailing edge and spanwise from tip to root. The lower temperatures near the root of each model are probably due to the effect of the parabolic-like stagnation-temperature profile. As indicated in the appendix of reference 2, the maximum stagnation temperature near the center of the jet airstream can exceed the temperature at the edge by approximately 100° F.

Temperature histories for the solid leading edge and for the skin and web combination just forward of the midchord, for test runs 2 and 3 on model MW-2-(2), were calculated in a manner similar to that employed in reference 2 (calculation B). In the calculations the structure was assumed to be integral and hence joint effects were neglected. Values

of the heat-transfer coefficients used in the calculations were deter-
mined from local flow conditions and Stanton numbers which were calcu-
lated by using the turbulent theory presented by Van Driest in refer-
ence 5 for values of skin temperature equal to the local stream
temperature. Values of the adiabatic-wall temperature used in the
calculations were obtained by using local flow conditions and turbulent
recovery factors (cube roots of the Prandtl numbers as determined by
local stream temperatures). The results, in the form of temperature
distributions at 3 and 8 seconds, are presented for the leading-edge
section in figure 8 and for the skin and web combination in figure 9,
with the corresponding experimental values.

Figures 8 and 9 indicate that the overall agreement between calcu-
lated and experimental temperatures is, in general, fairly good although
the interior temperatures in the thickest part of the solid leading-edge
section are lower than those predicted by theory. The lower test temper-
atures in this section are probably caused by the joint between the skin
and the solid leading-edge section which restricts the flow of heat from
the skin to the interior.

Stanton Number

Test values of Stanton number were determined from local flow con-
ditions and from experimentally determined heat-transfer coefficients
for each of the skin thermocouple locations not influenced by heat con-
duction and not in a region of low stagnation temperature. The experi-
mental heat-transfer coefficients were obtained by the method of refer-
ence 1 wherein the coefficient at a given location is assumed to be a
constant during the period of test conditions. The Stanton numbers are
plotted against local Reynolds numbers in figure 10 for all the hot runs
on models MW-2-(2) and MW-2-(3).

Theoretical values of Stanton number were obtained by use of local
Reynolds numbers and Mach numbers from the turbulent-flow method pre-
sented by Van Driest in reference 5. Van Driest's method for calcu-
lating the Stanton number assumes that the heat-transfer coefficient is
a function of the skin temperature and, hence, that the heat-transfer
coefficient varies during a test. By calculating values of Stanton
number for the skin temperature equal first to the local stream temper-
ature and then to the local adiabatic wall temperature, a band is formed
which encompasses the assumption of a constant heat-transfer coefficient
embodied in the experimentally determined Stanton number and within which
the experimental Stanton numbers should fall if good agreement between
theory and test is to be obtained. Since the majority of the experi-
mental data pertain to an angle of attack of $0°$, the theoretical data
are presented only for this angle of attack. A change in angle of attack

of $\pm 2^{\circ}$ results in a change of approximately ± 2 percent in the theoretical Stanton number. The effect of the painted model surface on the heat-transfer coefficient is believed to be negligible (ref. 3) and hence was not included in any of the calculations.

As indicated in figure 10, values of Stanton number determined from experimental heat-transfer coefficients are in fair agreement with the theoretical values. The probable error in the test values of Stanton number was estimated to be ± 5 percent.

Model Pressures

Experimental and theoretical pressure distributions on model MW-2-(3) are compared in figures 11 and 12 for an angle of attack of 0° and in figures 13 and 14 for an angle of attack of -2°. Experimental pressure distributions in the form of pressure coefficients are arbitrarily shown for only one time, 5 seconds, since the pressure coefficient is essentially a constant during the period of test conditions. Based on the probable error in the measured pressures, the pressure coefficients determined from the miniature differential gages may be in error by ± 0.010 and, from the other gages, by ± 0.002. Theoretical pressure distributions were calculated by using second-order, small-perturbation theory, with the pressures in the region influenced by the wing tip modified in accordance with the method of reference 4.

Except for the trailing-edge pressure coefficients at stations $9\frac{7}{8}$ and $15\frac{7}{8}$ inches from the tip, which were affected by interference of the bow waves off the probes with the shock waves from the trailing edge of the model, the calculated and experimental pressure-coefficient distributions are in fair agreement for both tests.

Model Strains

The purpose of instrumenting the models with wire strain gages was to obtain data on the phasing and frequency of model vibrations and possibly to obtain some data on the distribution and magnitude of the thermal stresses. Although the amplitudes of vibratory strains were damped considerably beyond 60 cycles per second (at 220 cycles per second the amplitude indicated by the gages was only about 0.2 true amplitude), the wire strain gages are believed to have yielded reliable frequency and phasing information. However, because of strain-gage failure after the first two tests on model MW-2-(2), phasing information concerning the flutter of this model was obtained from the motion pictures.

The EBDF-7D gages are temperature-compensated between 50° F and 250° F; however, beyond 250° F, in addition to the true strain transmitted from the structure, the gages experience a large indicated strain which is due solely to the increase in temperature. Hence, in order to obtain the true strain, a correction must be made whenever the gage temperature exceeds 250° F. This correction, which is difficult to assess accurately under the aerodynamic test conditions, is especially large at temperatures above 300° F, a temperature which most of the gages exceeded during the hot runs. Furthermore, in order to convert the true strains to stresses, especially in the skin, a two-dimensional state of stress should be assumed and, although gages were placed at right angles to each other for this purpose at three locations on model MW-2-(2), strain-gage failure was such that results were obtainable at only two of these stations, and then only for the cold run and part of the first hot run. Because of these and other uncertainties involved in obtaining stresses from the strain data, no stress data are presented.

Behavior of Model MW-2-(2)

Runs 1 to 5.- The first five runs on model MW-2-(2) consisted of four tests at an angle of attack of 0°, including one cold run, and one at an angle of attack of -2°. The first test was run cold to see if the failure of the original model MW-2 was due entirely to thermal stresses; however, since model MW-2-(2) survived the cold test and four of the following hot tests, the results are inconclusive.

At random intervals during run 1, the cold run, and then on run 2 shortly before the end of test conditions, beginning at 10.7 seconds and lasting for about 0.9 second, the model experienced small-amplitude torsional flutter at 120 cycles per second. Starting at 10.2 seconds, about 1.5 seconds before the end of test conditions on run 3, the model fluttered for 1.3 seconds with large amplitudes at 240 cycles per second; the front half of the model (from the root to within 2 inches of the tip) fluttered in phase with the last quarter of the model (from the tip to within 2 inches of the root) while the tip pivoted about a point close to the trailing edge. The greatest deflections appeared to occur at the leading edge. Approximately 0.2 second before the end of test conditions the flutter became torsional.

During the test at an angle of attack of -2°, run 4, the model experienced small-amplitude flutter at a frequency of approximately 360 cycles per second throughout the period of test conditions; however, because flutter was present before the model had experienced substantial temperature increases and because the characteristics of the flutter remained essentially constant throughout test conditions, aerodynamic heating apparently did not cause or influence the flutter.

Again, on run 5 at an angle of attack of 0°, the model fluttered at
a frequency of 230 cycles per second in the same manner as on run 3, but
in this test the flutter started at 8.8 seconds, 2.6 seconds before the
end of test conditions, and continued on into the shutdown phase. The
fact that flutter of this type was not present during the first hot run
at an angle of attack of 0° (run 2) but was present on the second and
third hot runs at an angle of attack of 0° (runs 3 and 5) might indicate
a reduction in model stiffness possibly incurred by loosening of some of
the riveted joints. This type of flutter was probably brought about by
a reduction in effective stiffness due to thermal stresses induced by
aerodynamic heating and a change in material properties due to the tem-
perature level.

Model MW-2-(2), a copy of model MW-2 and tested under similar aero-
dynamic conditions, was expected to behave similarly; at an angle of
attack of 0° model MW-2 experienced a partial dynamic failure brought
on by aerodynamic heating which caused a reduction in stiffness of the
model, skin buckling, and flutter (see ref. 2). The fact that
model MW-2-(2) did not behave in such a manner and survived all tests
at an angle of attack of 0° even though it was subjected to higher test
temperatures probably indicates that the thermal stresses due to the
nonuniform temperature distribution were smaller in model MW-2-(2) than
in model MW-2.

The thermal stress at any point in the structure is, in part, a
function of the difference in the temperature at that point and the
average temperature of the structure. Because the average temperature
was not available, the difference between the maximum temperature in
the skin and the minimum temperature in the web, an indication of the
thermal stress, was obtained for the same skin and web combination for
the two models. The maximum skin and minimum web temperatures are pre-
sented in figure 15(a) and the temperature differences are presented
in figure 15(b). Although shown for only one skin and web combination,
the results are typical of those obtained elsewhere in the models. As
shown in this figure, model MW-2-(2) experienced considerably smaller
temperature differences from skin to web and, consequently, smaller
thermal stresses than model MW-2.

The larger temperature difference experienced by model MW-2 was
apparently caused by lower joint conductivity. Although references 6
and 7 discuss some effects of joint conductivity on the temperatures
and thermal stresses in skin-stiffener combinations similar to those of
the multiweb wings, values of the necessary parameters obtained from the
tests were not in good agreement with those of either reference, espe-
cially reference 6. Thus, in order to obtain information as to the
magnitude of the thermal stresses involved, theoretical calculations for
the temperature distribution throughout the skin-web combination under
discussion were made in a manner similar to that used in reference 2

(calculation B), except that values of joint conductivity ranging from zero to infinity were used in the calculations. The curve of figure 16 for the maximum temperature difference as a function of joint conductivity was established from these calculations. The maximum temperature differences experienced by the two models would intersect the curve at the two locations shown; estimated thermal stresses for these two values of joint conductivity indicate that the maximum skin and web thermal stresses for model MW-2 were approximately 10 and 34 percent, respectively, above the corresponding stresses for model MW-2-(2). The approximate manner in which these stresses were obtained and the fact that they are based on various simplifying assumptions indicate that the values given merely reflect the overall relative magnitude or intensity of the induced thermal stresses. It can be seen, however, that joint conductivity has a definite effect on the thermal stresses and therefore on the effective stiffness of a structure.

Run 6 (failure).- The failure of model MW-2-(2) occurred during run 6 at an angle of attack of 2°. At approximately 1.9 seconds, or about 0.2 second after the beginning of test conditions, the model began to flutter with small amplitudes at frequencies between 360 and 400 cycles per second. The model continued to flutter in this frequency range and in an upright postion after 1.9 seconds until failure occurred at 8.59 seconds. The motion pictures indicate that during this period a buckle gradually developed in the skin near the root and that prior to failure the buckle extended over about the central third of the chord. At 8.59 seconds the model wrinkled completely across the chord near the root (just above the aerodynamic fence) and collapsed to a position such that the model made about a 30° angle with the fence, as shown in figure 17.

The failure of the model was probably the result of a combination of factors. The repeated testing wherein the model had undergone violent vibrations during the starting and shutdown phases of the jet had a tendency to weaken the structure. In addition, because of the amount and direction of built-in twist, model MW-2-(2) was subjected to root-bending stresses approximately 9 percent higher at an angle of attack of 2° than at -2°. Although the model fluttered until failure, the flutter was not violent and probably contributed very little to the failure. Superimposed on these conditions was aerodynamic heating, with the accompanying reduction in effective stiffness due to thermal stresses induced by the nonuniform heating and reduction in modulus of elasticity due to the temperature level.

Behavior of Model MW-2-(3)

Model MW-2-(3) was tested at angles of attack of 0° and -2° and survived both tests with no visible damage. Flutter was not apparent during test conditions at an angle of attack of 0°. However, starting

at 9.1 seconds, about 2.3 seconds before the end of test conditions for
the test at an angle of attack of -2°, the model fluttered for 2.5 seconds
with a high-frequency, small-amplitude nature and although the miniature
gages had been located in such a way as to obtain the frequency of model
vibrations, those recorded by these gages were of such random nature that
no frequencies could be obtained. Although not present until late in the
test and therefore probably the result of aerodynamic heating, this flut-
ter appeared to be the same as that experienced by model MW-2-(2) during
the two tests at an angle of attack; however, the flutter experienced by
model MW-2-(2) was evident from the beginning of test conditions and there-
fore was probably independent of any aerodynamic heating.

The miniature gages and pressure tubing located inside model MW-2-(3)
(fig. 4) undoubtedly added to the mass of the structure, probably changed
the effective stiffness, and thus affected the behavior of the model;
these factors may have been influential in the survival of this copy of
the MW-2-type wing.

CONCLUDING REMARKS

Eight tests were made on two duplicate aluminum-alloy multiweb wings,
models MW-2-(2) and MW-2-(3), in order to obtain additional information
on the behavior and failure of the original MW-2-type wing. These wings
were tested under aerodynamic conditions similar to those encountered in
supersonic flight at a Mach number of 2, and model temperatures, pressures,
and strains were measured with the following results:

The results of previous tests on the model MW-2 type structure indi-
cated that the model was a marginally safe structure in that modifying
the structure by using a light tip bulkhead would result in failure
whereas additional stiffness gained by using a thicker skin or a stronger
material, or by adding internal ribs would prevent failure. The tests
reported herein again indicate that the model is a marginally safe struc-
ture in that construction details, such as joint conductivity and
"built-in" twist, can also influence the safety.

Model MW-2-(2) survived five tests at angles of attack of 0° and -2°
before failing at an angle of attack of 2°, whereas the original model MW-2
failed dynamically at an angle of attack of 0°; the only apparent differ-
ence in the two models was in the thermal conductivity of the joints.
Model MW-2-(2) had higher joint conductivity than model MW-2, with the
result that the induced thermal stresses and resulting loss in effective
stiffness were smaller and allowed model MW-2-(2) to survive several
tests similar to the one in which model MW-2 failed.

Model MW-2-(2) failed statically at an angle of attack of 2° because of weakening of the structure brought about by repeated testing, stiffness losses caused by the aerodynamic heating, and aerodynamic loading. The failure occurred at an angle of attack of 2° instead of -2° because "built-in" twist in the model caused the aerodynamic loads to be about 9 percent higher at the positive angle of attack.

Model MW-2-(3), whose mass and stiffness were affected by the pressure gages and tubing inside the model, survived hot runs at angles of attack of 0° and -2° with no visible damage.

During seven of the eight tests the models experienced aerodynamic heating. Calculated temperature distributions in the leading-edge section and in one skin and web combination for runs 2 and 3 of model MW-2-(2) showed good agreement with the experimental temperatures. Stanton numbers calculated by using the turbulent theory presented by Van Driest were in fair agreement with the values of the Stanton numbers determined from the experimental heat-transfer coefficients of the seven hot tests.

Calculated pressure distributions, based on second-order, small-perturbation theory, with modifications made to the pressures in the region influenced by the wing tip, were in good agreement with the experimental pressure distributions on model MW-2-(3).
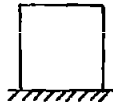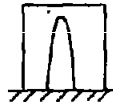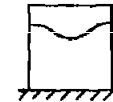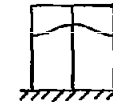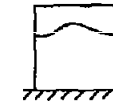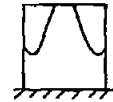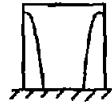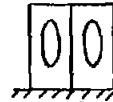
Strain data could be used only to provide frequency and phasing information and to help reconstruct model behavior.

Langley Aeronautical Laboratory,
    National Advisory Committee for Aeronautics,
        Langley Field, Va., August 6, 1957.

REFERENCES

1. Heldenfels, Richard R., Rosecrans, Richard, and Griffith, George E.:
   Test of an Aerodynamically Heated Multiweb Wing Structure (MW-1)
   in a Free Jet at Mach Number 2. NACA RM L53E27, 1953.

2. Griffith, George E., Miltonberger, Georgene H., and Rosecrans, Richard:
   Tests of Aerodynamically Heated Multiweb Wing Structures in a Free
   Jet at Mach Number 2 - Two Aluminum-Alloy Models of 20-Inch Chord
   With 0.064- and 0.081-Inch-Thick Skin. NACA RM L55F13, 1955.

3. Rosecrans, Richard, Vosteen, Louis F., and Batdorf, William J., Jr.:
   Tests of Aerodynamically Heated Multiweb Wing Structures in a Free
   Jet at Mach Number 2 - Three Aluminum-Alloy Models and One Steel
   Model of 20-Inch Chord and Span With Various Internal Structures
   and Skin Thicknesses. NACA RM L57H01, 1957.

4. Czarnecki, K. R., and Mueller, James N.: An Approximate Method of
   Calculating Pressures in the Tip Region of a Rectangular Wing of
   Circular-Arc Section at Supersonic Speeds. NACA TN 2211, 1950.

5. Van Driest, E. R.: Turbulent Boundary Layer in Compressible Fluids.
   Jour. Aero. Sci., vol. 18, no. 3, Mar. 1951, pp. 145-160, 216.

6. Griffith, George E., and Miltonberger, Georgene H.: Some Effects
   of Joint Conductivity on the Temperatures and Thermal Stresses in
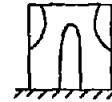   Aerodynamically Heated Skin-Stiffener Combinations. NACA TN 3699,
   1956.

7. Dukes, W. H., and Schnitt, A.: Structural Design for Aerodynamic
   Heating. Part I - Design Information. WADC Tech. Rep. 55-305,
   Pt. I (Bell Aircraft Corp., Contract No. AF33(616)-2581),
   Wright Air Dev. Center, U. S. Air Force, Oct. 1955.

TABLE I.- NATURAL MODES AND FREQUENCIES OF MW-2 TYPE MODELS

Model	Frequency, cps, for node line[a] -						
	A	B	C	D	E	F	G
MW-2-(2)	68 60	143 139	---- ----	264 248	---- ----	337 317	---- ----
MW-2-(3)	59	138	194	----	250	----	348
MW-2-(4)	69	147	----	274	----	346	----
MW-2-(5)	70	146	----	269	----	347	----

Model	Frequency, cps, for node line[a] -						
	H	I	J	K	L	M	N
MW-2-(2)	402 377	---- 423	---- 493	517 517	---- 545	651 ----	---- 675
MW-2-(3)	392	----	473	----	----	623	----
MW-2-(4)	413	450	----	535	585	665	735
MW-2-(5)	383	449	----	526	577	648	713

[a]Modes shown are composites from modes for all models. Individual modes varied slightly from those shown.

TABLE II.- AERODYNAMIC TEST DATA

[Mach number, 1.99]

Test		Angle of attack, deg	Stagnation pressure, lb/sq in. abs	Stagnation temperature, °F	Free-stream static pressure, lb/sq in. abs	Free-stream dynamic pressure, lb/sq in.	Free-stream temperature, °F	Free-stream velocity, fps	Free-stream density, slugs/cu ft	Speed of sound, fps	Reynolds number per foot, 1/ft
Model	Run										
MW-2-(2)	1	0	101	89	13.2	36.4	-154	1.70×10^3	3.61×10^{-3}	0.86×10^3	25.7×10^6
	2	0	117	540	15.2	42.0	98	2.30	2.29	1.16	13.3
	3	0	114	503	14.8	41.1	77	2.26	2.32	1.14	13.6
	4	-2	115	517	15.0	41.5	85	2.28	2.30	1.14	13.5
	5	0	114	474	14.8	40.9	61	2.23	2.38	1.12	14.1
	6	2	116	525	15.1	41.8	90	2.29	2.30	1.15	13.4
MW-2-(3)	1	0	115	489	14.9	41.3	70	2.24	2.36	1.13	13.9
	2	-2	114	518	14.8	41.0	86	2.28	2.28	1.14	13.3

TABLE III.- TEMPERATURES FOR MODEL MW-2-(2)

Temperature, °F, at thermocouple -

Run	t, sec	1	2	3	4	5	6	7	9	10	11	13	14	15	16	17	18	19	20	21	22	23	26	27	28	29	30
2	0	77	77	77		79	83	79	82	79		80		80	80	76	84	79	82	77	76		85	79	83	78	77
	1	138	107	90		130	129	135	125	127		123		104	81	76	120	115	122	107	100		119	112	113	104	96
	2	249	186	136		203	211	212	197	195		187		150	94	87	186	182	184	156	148		188	178	174	146	145
	3	339	266	202		265	285	283	261	260		247		198	123	109	242	231	242	198	188		234	222	214	178	180
	4	384	321	260		311	334	333	310	308		292		238	160	136	285	271	285	230	220		271	257	248	205	211
	5	413	362	308		346	371	367	346	343		326		275	202	166	320	302	320	254	246		303	287	277	225	240
	6	431	390	346		374	397	393	374	372		354		308	240	193	349	328	348	273	267		329	313	301	242	265
	7	446	412	376		396	417	411	397	393		375		336	275	219	370	348	370	289	281		351	333	322	255	288
	8	455	428	398		413	431	426	412	408		392		359	306	242	389	364	388	300	294		369	351	340	268	308
	9	463	440	416		425	442	436	425	420		406		377	332	261	405	376	402	309	304		384	366	355	277	325
	10	467	448	428		436	449	444	434	429		416		391	354	278	416	388	414	316	314		397	378	370	286	341
	11	469	453	437		444	457	451	441	434		422		405	373	294	426	398	421	322	322		408	388	382	291	357
	12	472	459	444		447	460	451	445	439		427		413	387	307	431	403	427	327	328		416	397	390	298	369
	13	472	461	450		451	461	453	447	441		431		419	398	316	433	409	430	329	319		426	408	404	299	383
	14	471	463	452		452	454	454	443	442		436		426	407	323	433	407	434	325	315		424	405	402	295	393
	15	467	462	453		451	448	453	438	439		432		428	415	330	430	404	432	324	316		419	403	398	296	395
3	0	80	78	79	78	81	86	85	81	81	80	82	81	80	75	75	81	74	82	78	73	76	80	73	77	74	72
	1	135	106	87	86	129	125	134	123	126	93	122	116	100	77	76	115	109	118	105	96	76	111	108	106	99	90
	2	240	180	132	122	197	201	205	193	190	131	182	171	139	89	85	180	175	176	147	135	85	176	174	167	135	136
	3	320	253	193	178	256	271	270	254	250	178	238	221	183	117	105	232	226	229	187	172	102	221	217	209	164	170
	4	364	305	249	232	300	321	316	301	294	221	282	262	223	154	129	274	265	271	215	199	122	258	252	243	188	199
	5	391	342	295	278	335	357	351	337	329	260	316	295	259	192	156	306	297	303	239	222	147	289	281	273	213	228
	6	411	371	330	317	363	384	375	365	356	294	343	323	292	229	181	334	323	331	257	240	170	315	306	298	235	252
	7	425	391	358	347	384	404	394	386	376	322	365	346	319	263	205	357	344	355	272	254	191	337	327	320	247	274
	8	437	409	382	373	404	419	413	402	392	345	382	366	342	293	225	370	361	370	283	265	213	355	344	338	262	293
	9	445	422	400	393	416	431	420	413	405	365	396	382	360	318	244	389	376	384	294	276	231	371	360	354	262	310
	10	452	432	413	408	425	440	429	423	414	385	402	398	380	344	265	405	390	399	300	284	245	383	371	367	264	326
	11	455	438	422	423	440	448		434		400		410	389	360	274	411	399	411	306	290	260	393	381	379	271	339
	12	457	443	431	429	440	449		437		405		416	397	373	286	416	403	411	309	295	272	401	388	388	275	350
	13	458	446	436	435	443	451		440		413			406	385	297	422	409	416	310	289	284	410	398	401	278	365
	14	455	447	439	439	445	453		441		417			411	395	303	426	412	419	302	282	292	415	404	406	273	375
	15	454	448	441	442	445	443		431		420			414	402	310	430	419	417	303	283	299	406	396	397	276	379
4	0	81	83	82	80	84					85	86	86			79	88			81	78	80				81	79
	1	144	117	96	91	134					98	124	108			81	121			111	104	83				106	97
	2	249	196	144	130	201					127	172	143			89	183			153	147	90				139	143
	3	335	270	208	190	261					170	222	186			108	233			190	185	111				172	180
	4	380	321	264	243	305					214	262	227			134	273			221	217	137				194	210
	5	406	359	311	291	338					252	294	261			162	305			241	238	162				211	235
	6	425	384	347	330	368					286	321	291			188	331			260	255	189				226	259
	7	439	405	375	362	392					316	345	319			213	354			275	270	213				239	280
	8	447	423	397	387	409					340	363	340			236	370			286	280	232				250	
	9	456	434	415	406	422					364	380	360			257	388			296	287	252				258	
	10	460	442	427	419	432					380	393	375			273	398			303	296	269				264	
	11	463	449	437	432	441					395	404	389			289	408			308	304	282				270	
	12	465	452	445	440	446					405	411	400			301	415			311	310	294				273	
	13	466	455	450	446	449					413	417	408			311	422			314	309	303				273	
	14	465	456	454	450	454					420	422	414			319	419			307	306	311				275	
	15	459	455	453	451	450					424	423	417			326	417			306	307	316				277	
5	0	74	74	72		77					76			79	78		78			75	73			72			73
	1	121	102	84		122					89			110	96		112			101	75			93			95
	2	214	170	125		186					123			169	134		161			140	81			125			128
	3	292	237	182		243					165			215	172		207			174	94			152			160
	4	327	284	231		285					206			252	207		244			201	111			175			185
	5	352	317	272		318					241			281	237		274			221	131			190			204
	6	371	343	304		346					272			307	266		300			238	151			206			220
	7	384	363	330		370					299			326	291		321			253	172			218			233
	8	393	377	350		388					322			342	311		339			263	190			229			244
	9	402	389	366		408					342			357	330		354			272	207			237			252
	10	408	398	378		422					357			366	343		365			278	222			244			260
	11		404	387							364			376	356		375			282	237			248			265
	12		409	394							381			382	365		381			286	247			250			269
	13		411	398							389			386	371		385			284	260			248			263
	14		413	401							395			385	377		389			281	268			248			260
	15		412	402							397			381	380		389			280	275			246			260
6	0		73	73							77			79	78					76	74			74			73
	1		103	85							90			112	96					107	75			98			97
	2		183	132							130			178	134					161	83			144			136
	3		262	198							186			237	186					204	107			182			175
	4		316	256							237			280	230					238	135			211			204
	5		355	302							282			315	268					264	164			236			229
	6		385	339							319			344	301					284	192			255			245
	7		404	367							349			366	328					300	218			270			261
	8		421	390							374			384	351					312	240			283			272

TABLE IV.- TEMPERATURES FOR MODEL MW-2-(3)

Run	t, sec	Temperature, °F, at thermocouple -										
		1	2	3	4	5	6	8	9	10	11	12
1	0	84	75	79	85	84	78	76	85	76	79	73
	1	131	105	84	124	120	87	112	118	101	109	97
	2	202	155	88	189	176	104	175	180	140	171	131
	3	264	195	97	243	227	136	223	228	173	210	157
	4	308	227	116	286	263	168	261	267	202	243	180
	5	341	249	140	321	297	201	293	300	223	271	198
	6	365	266	168	348	324	236	318	327	240	294	212
	7	384	281	193	367	347	266	340	346	252	314	223
	8	398	290	219	384	364	291	357	363	265	330	235
	9	411	298	241	398	380	313	371	377	274	346	244
	10	419	306	261	407	391	332	382	388	280	358	251
	11	424	309	280	417	401	349	393	398	286	369	256
	12	426	310	298	421	407	362	399	404	291	378	256
	13	430	310	315	425	412	372	404	411	288	392	256
	14	419	306	330	418	408	384	399	404	284	387	256
	15	418	304	337	417	407	386	398	403	285	384	258
2	0	80	73	77	83	83	78	74	84	75	78	73
	1	128	106	82	121	118	84	112	119	100	105	97
	2	200	163	88	189	177	104	179	184	144	164	132
	3	263	212	98	242	225	132	234	231	181	202	162
	4	306	242	118	285	266	167	274	271	209	234	184
	5	340	269	141	318	298	201	308	301	232	261	204
	6	366	285	167	345	322	234	335	330	251	285	221
	7	387	300	194	368	346	267	359	352	264	307	232
	8	403	308	218	386	367	293	378	371	274	326	242
	9	415	318	240	400	382	317	391	382	284	341	252
	10	425	327	257	411	395	337	402	389	292	358	260
	11	431	331	275	421	·406	354	414	400	295	371	265
	12	435	331	291	426	415	370	416	407	298	380	262
	13	437	331	306	430	421	381	421	405	296	397	262
	14	429	323	330	423	414	391	416		293	391	265
	15	425	322	339	420	412	394	412		292	386	265
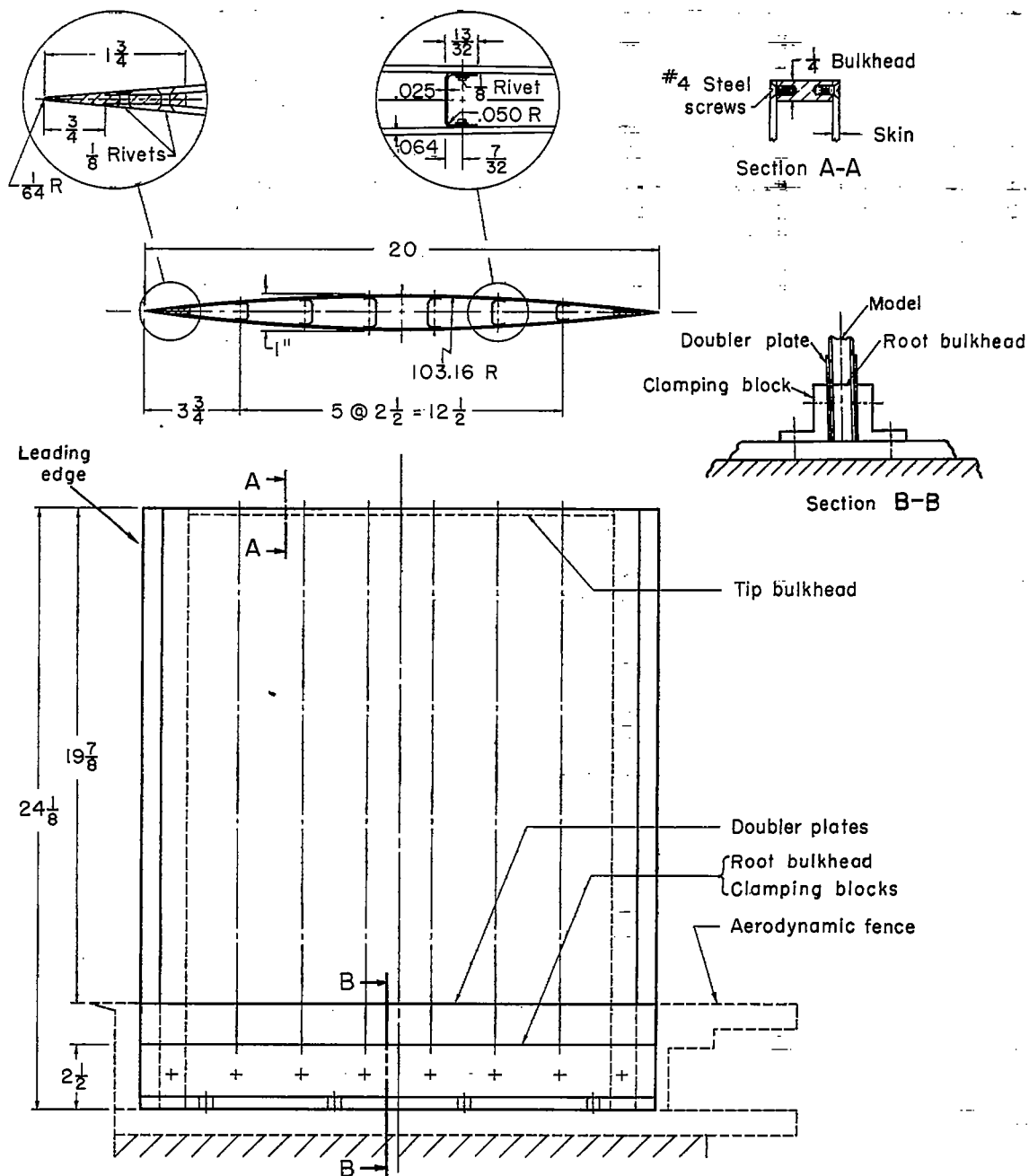
Figure 1.- Details of multiweb wing models MW-2-(2) and MW-2-(3).   All
dimensions are in inches.
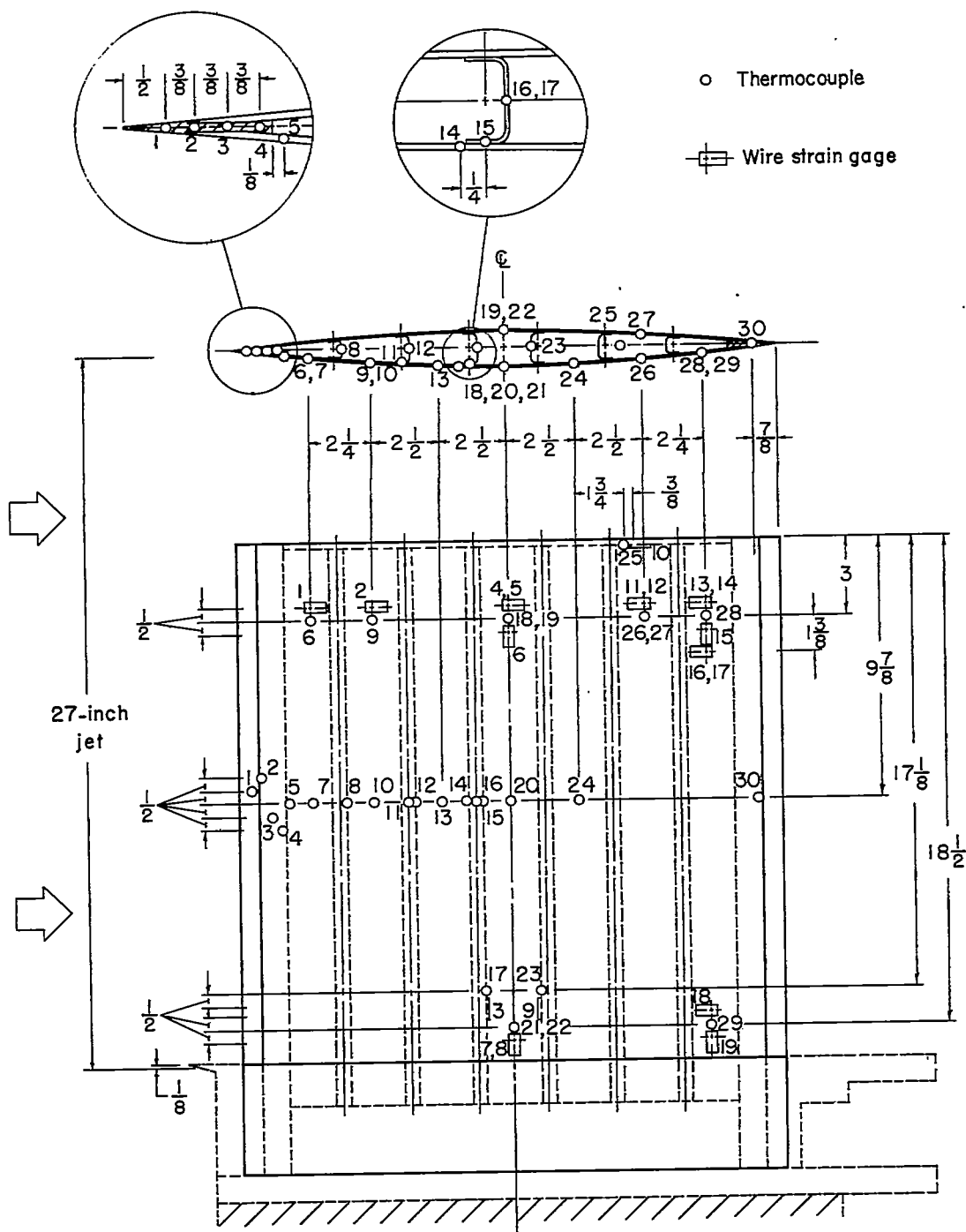
Figure 2.- Location of model MW-2-(2) instrumentation. (Wire strain gages 5, 8, 12, and 17 are on far skin; wire strain gage 14 is on outside of near skin.) All dimensions are in inches.
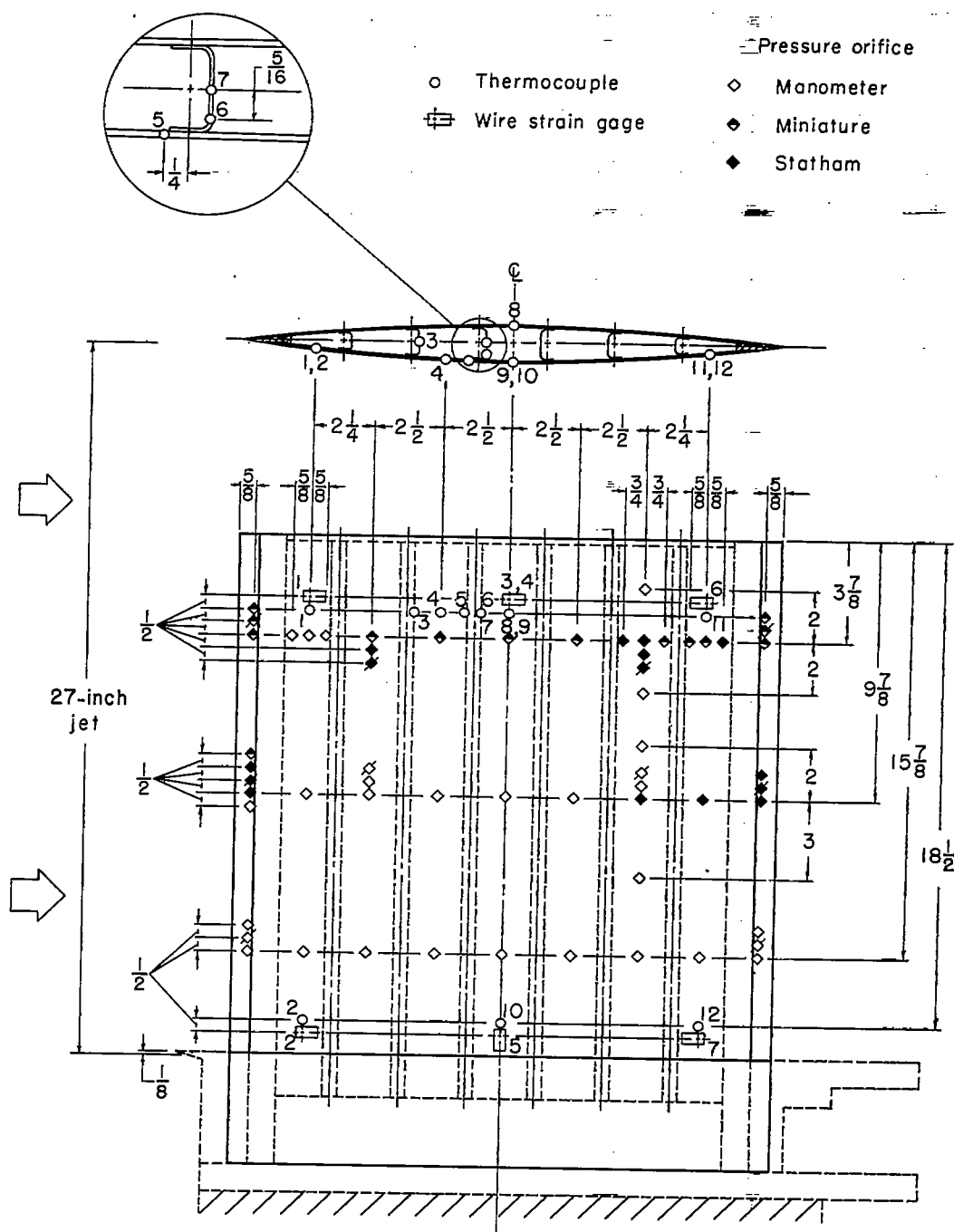
Figure 3.- Location of model MW-2-(3) instrumentation. (Wire strain gage 4 and pressure orifices with tick marks are on far skin.) All dimensions are in inches.
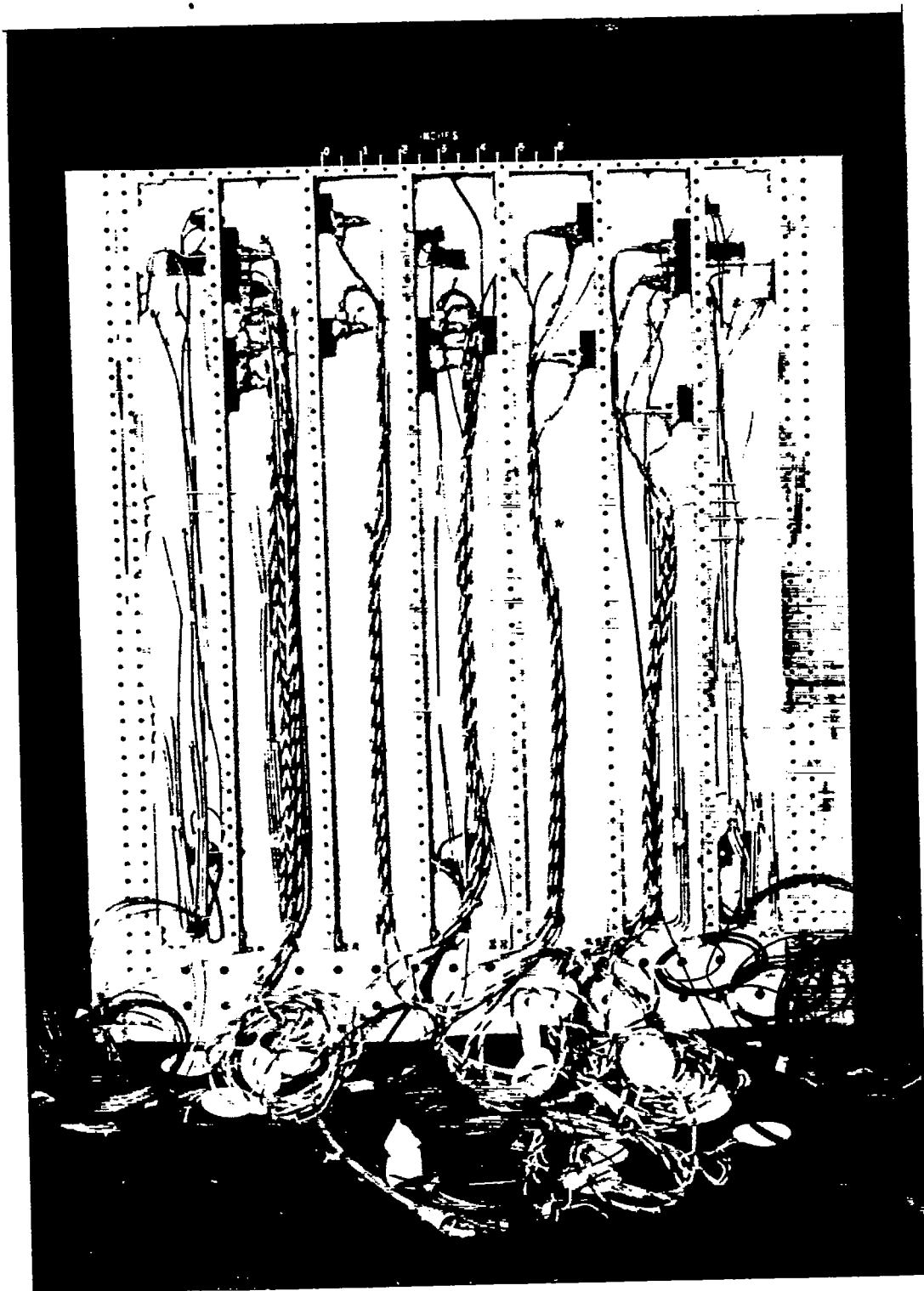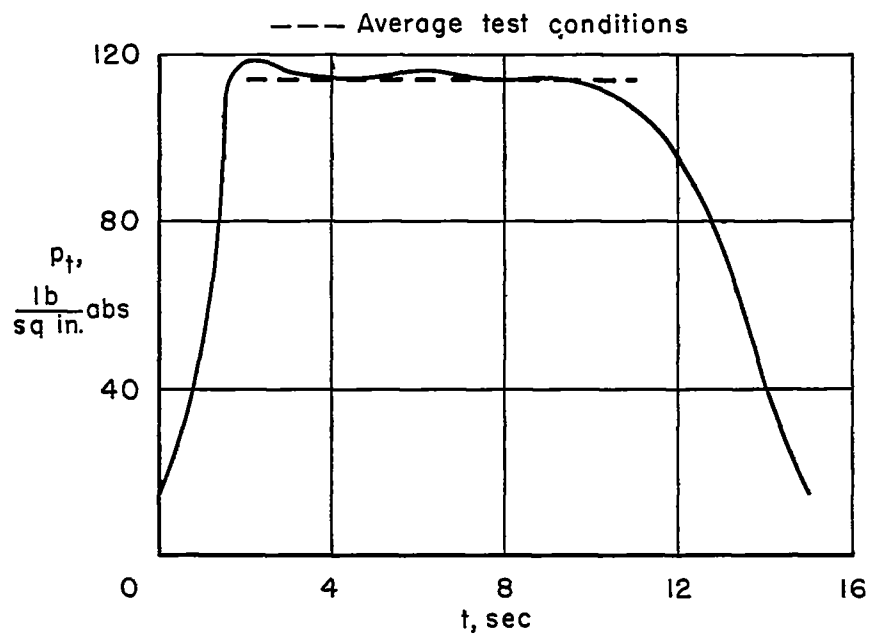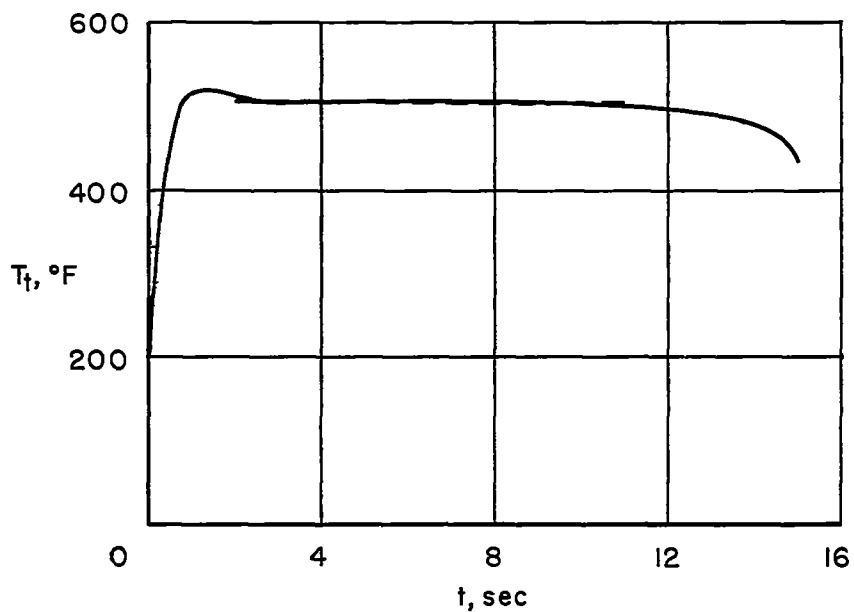
Figure 4.- View of model MW-2-(3) instrumentation.   L-83063

Figure 5.- Model in place at nozzle exit prior to test. (Stagnation-temperature probes can be seen behind model.)

L-81922

--- Average test conditions

(a) Stagnation pressure.

(b) Stagnation temperature.

Figure 6.- Typical histories of tunnel stagnation pressure and temperature.
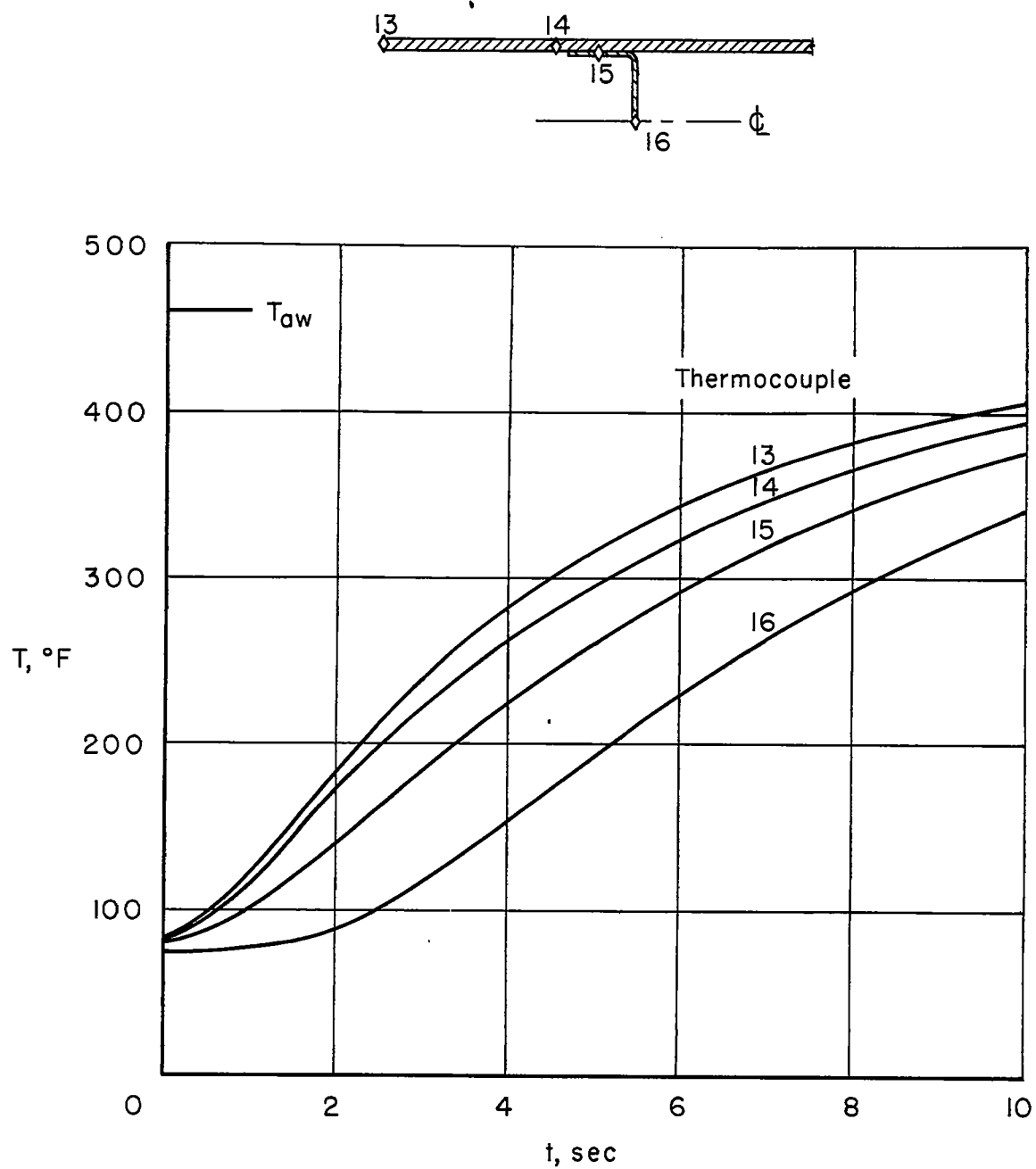
Figure 7.- Temperature histories of skin and web combination on model
MW-2-(2), run 3.
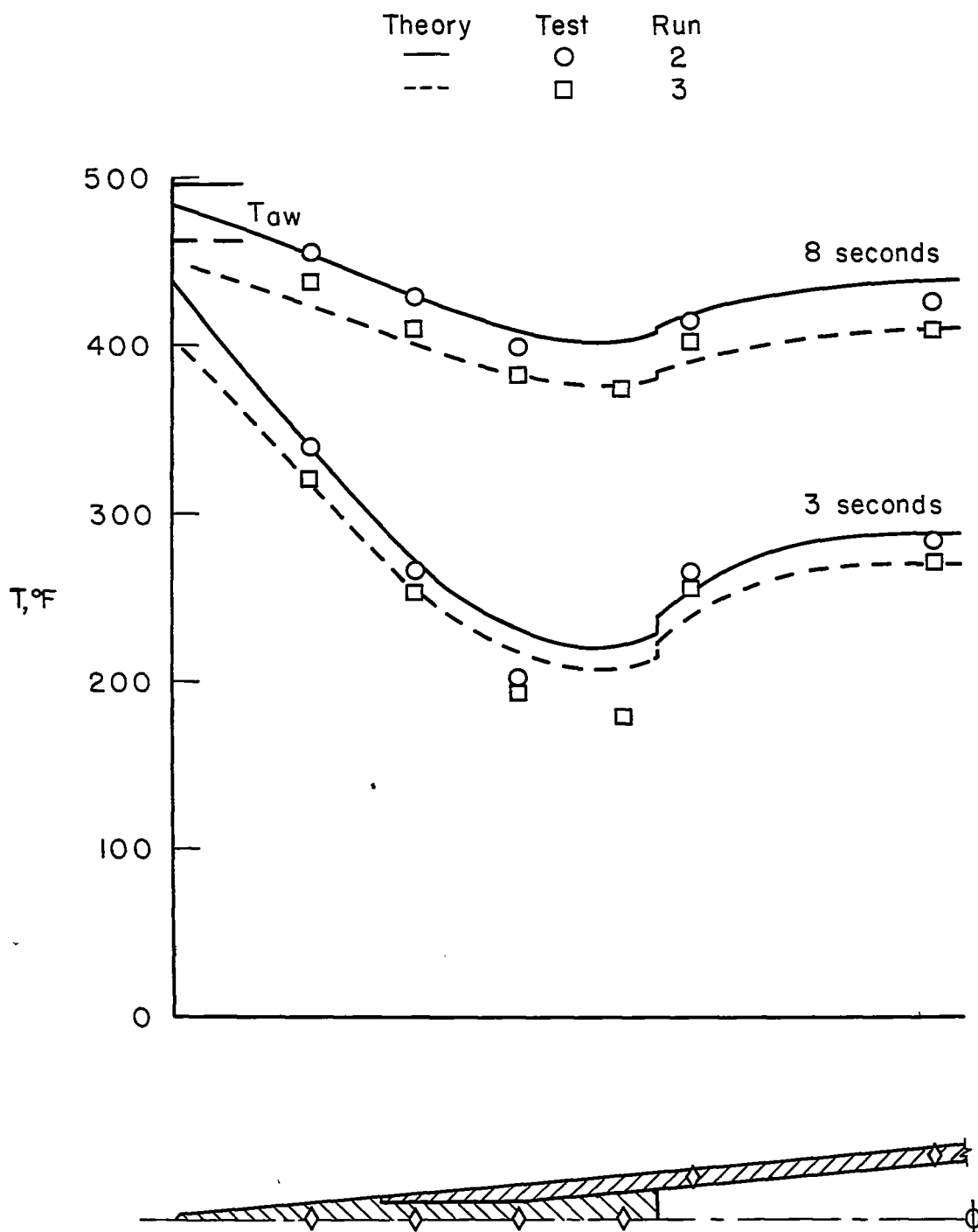
Figure 8.- Temperature distributions of leading-edge section on model MW-2-(2) at an angle of attack of 0°.
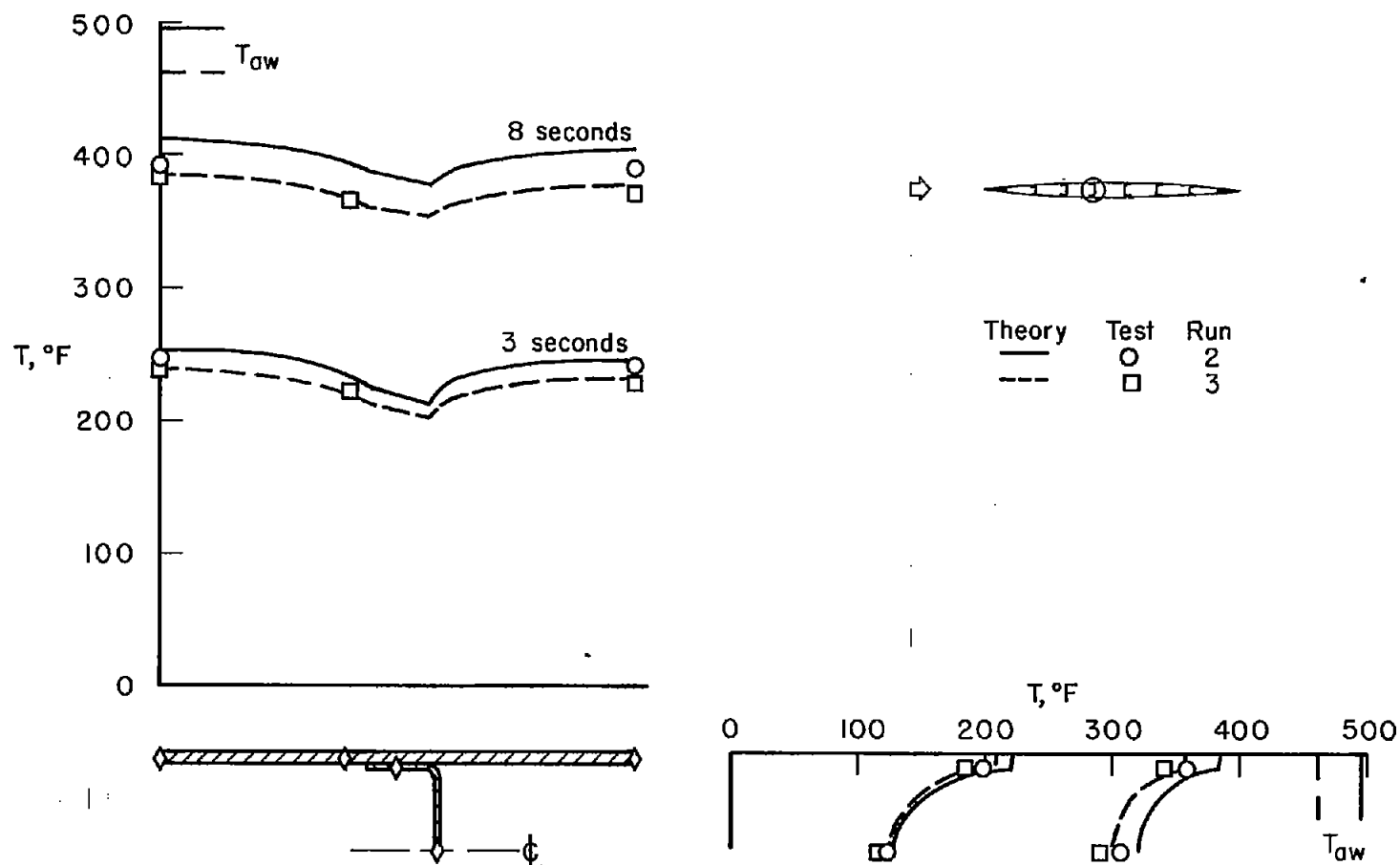
Figure 9.- Temperature distributions of skin and web combination on model MW-2-(2) at an angle of attack of 0°.
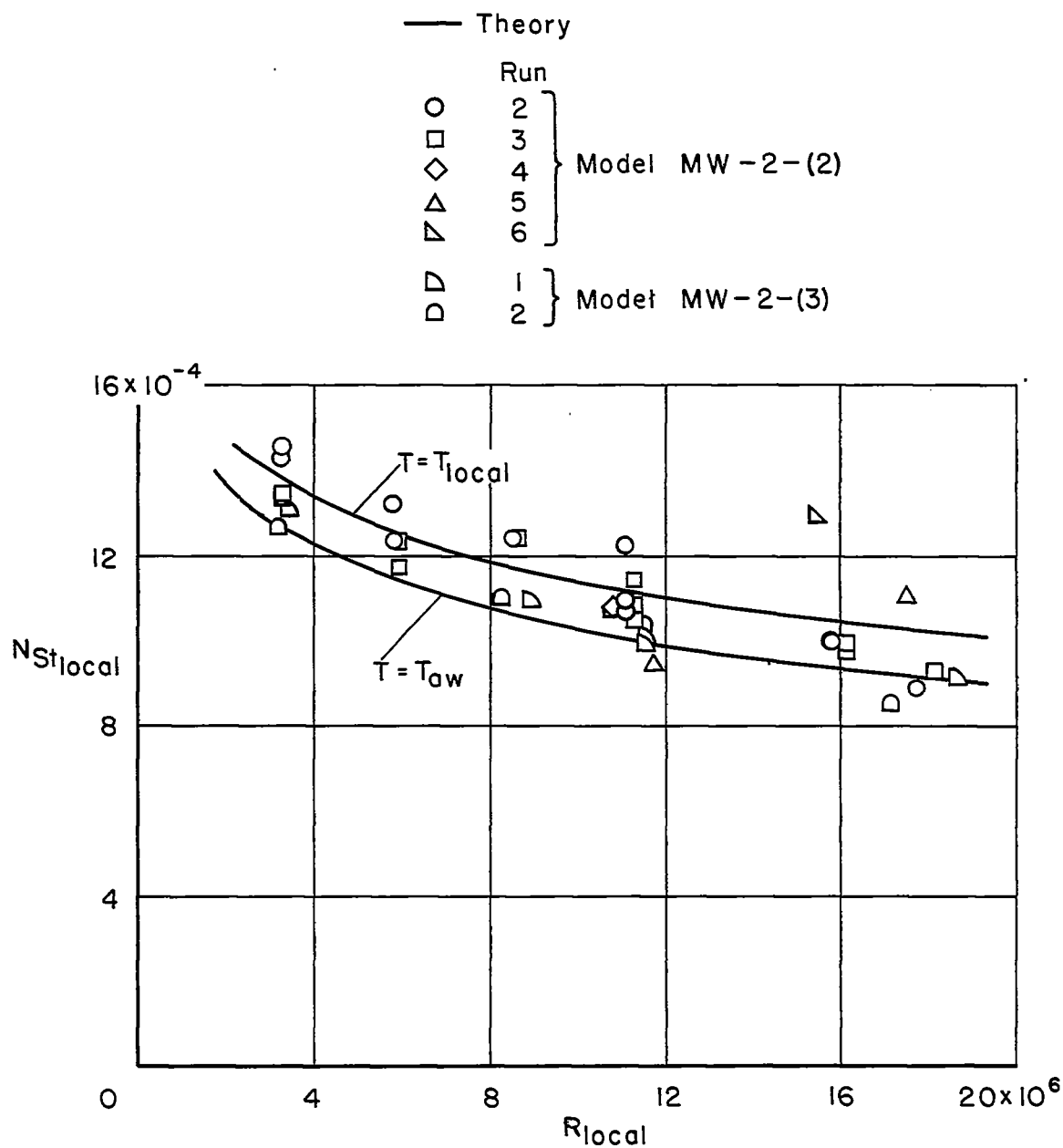
Figure 10.- Comparison of experimental Stanton numbers at angles of attack of $0°$, $-2°$, and $2°$ with theoretical Stanton numbers at an angle of attack of $0°$.

O Test
— Theory
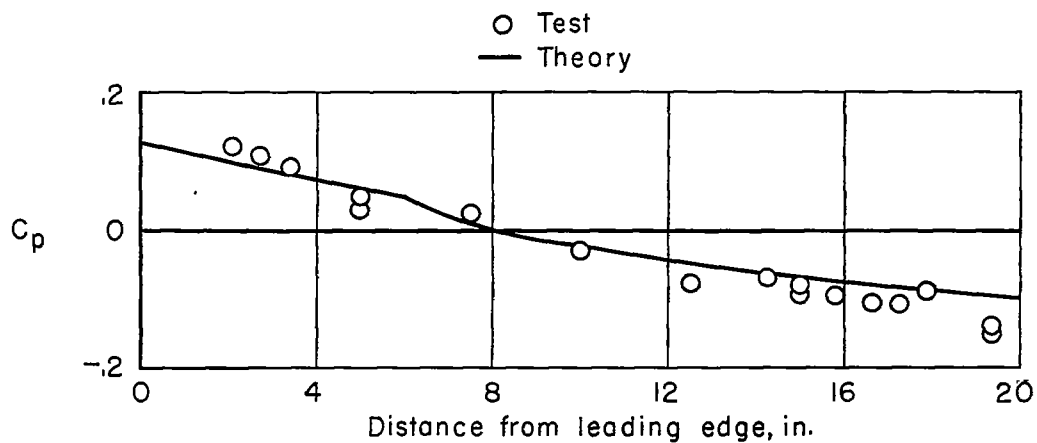
(a) 3-7/8 inches from model tip.

(b) 9-7/8 inches from model tip.

(c) 15-7/8 inches from model tip.

Figure 11.- Chordwise pressure-coefficient distributions on model
MW-2-(3) at an angle of attack of 0°.

O Test
—— Theory
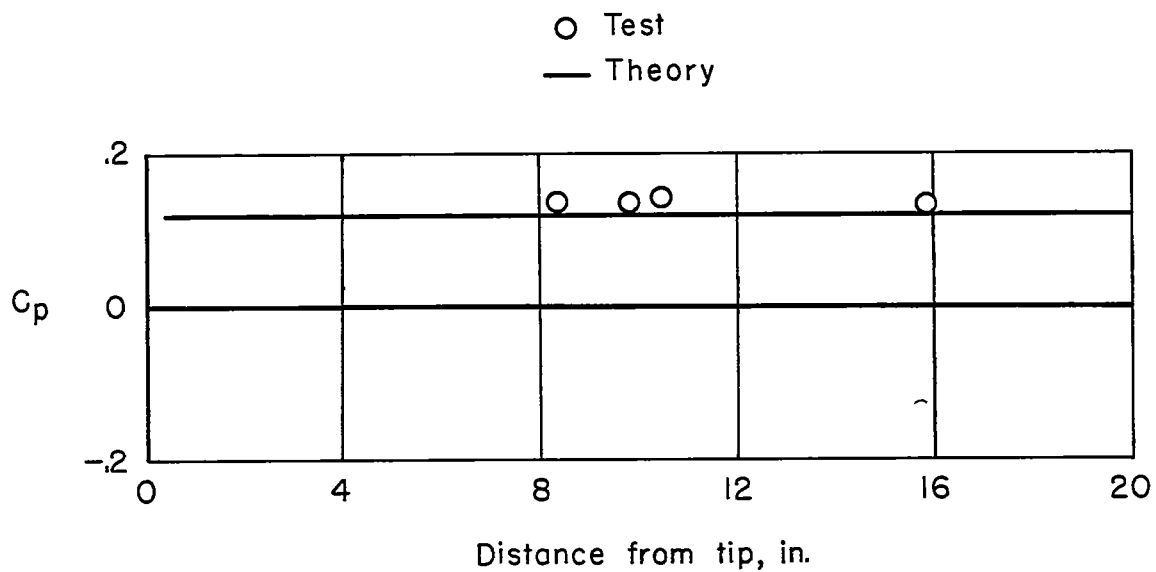
(a) 5/8 inch from leading edge.
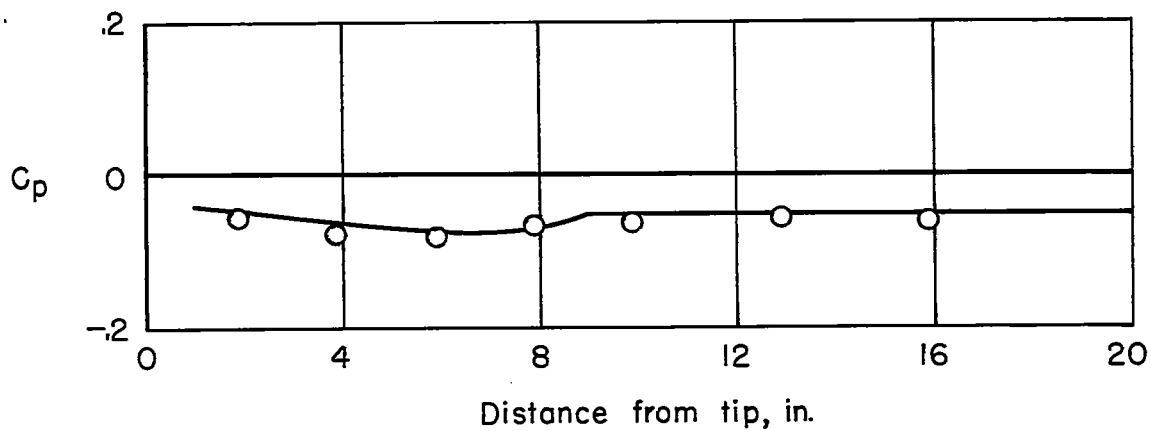
(b) 15 inches from leading edge.

Figure 12.- Spanwise pressure-coefficient distributions on model
MW-2-(3) at an angle of attack of 0°.
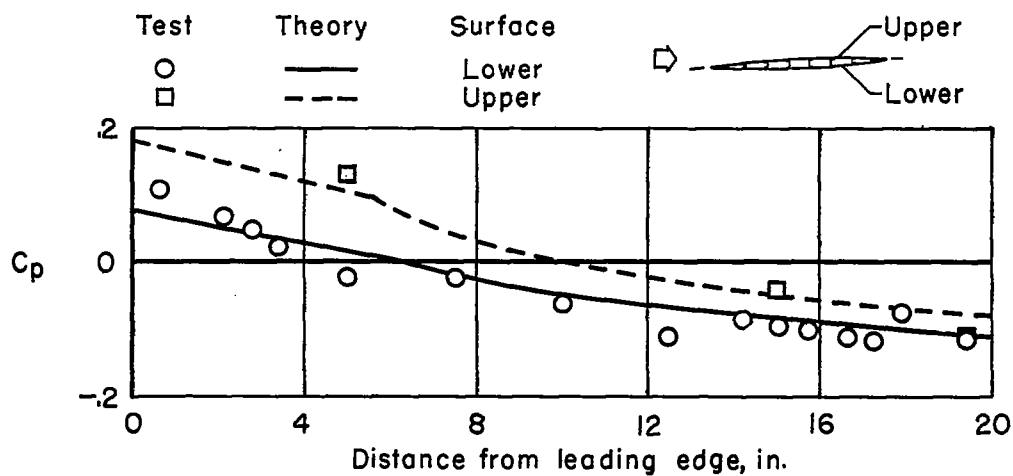
(a)   3-7/8 inches from model tip.
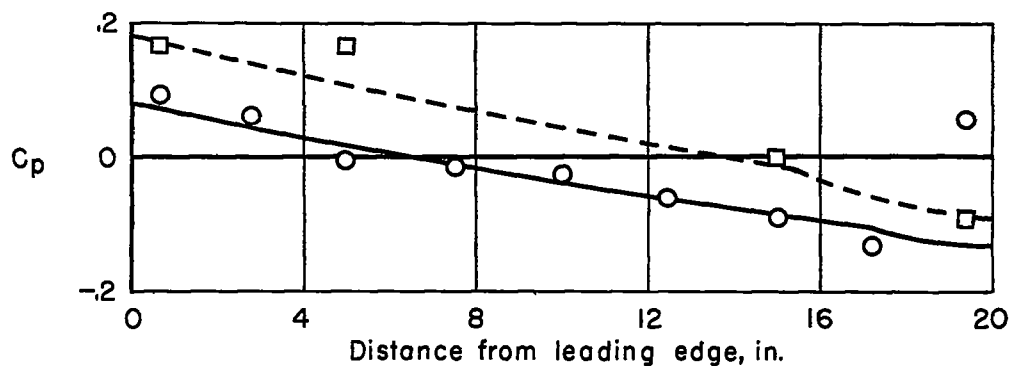
(b)   9-7/8 inches from model tip.
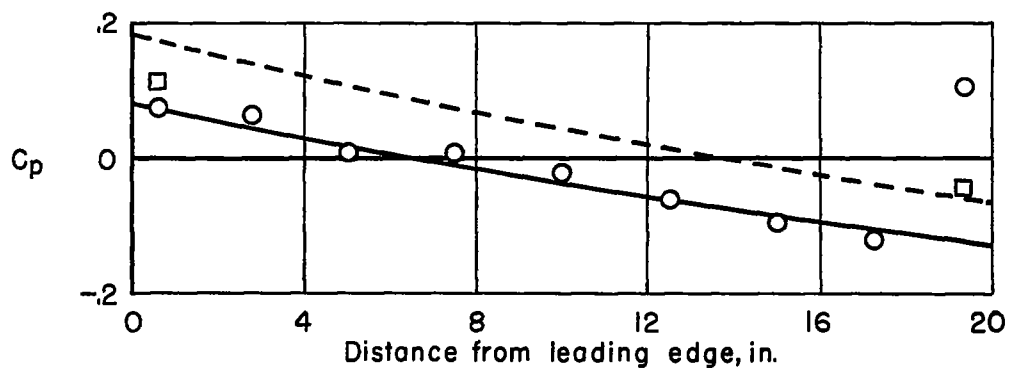
(c)   15-7/8 inches from model tip.

Figure 13.- Chordwise pressure-coefficient distributions on model
MW-2-(3) at an angle of attack of -2°.

Test   Theory   Surface   ⇨ ─── Upper
  O   ─────   Lower   Lower
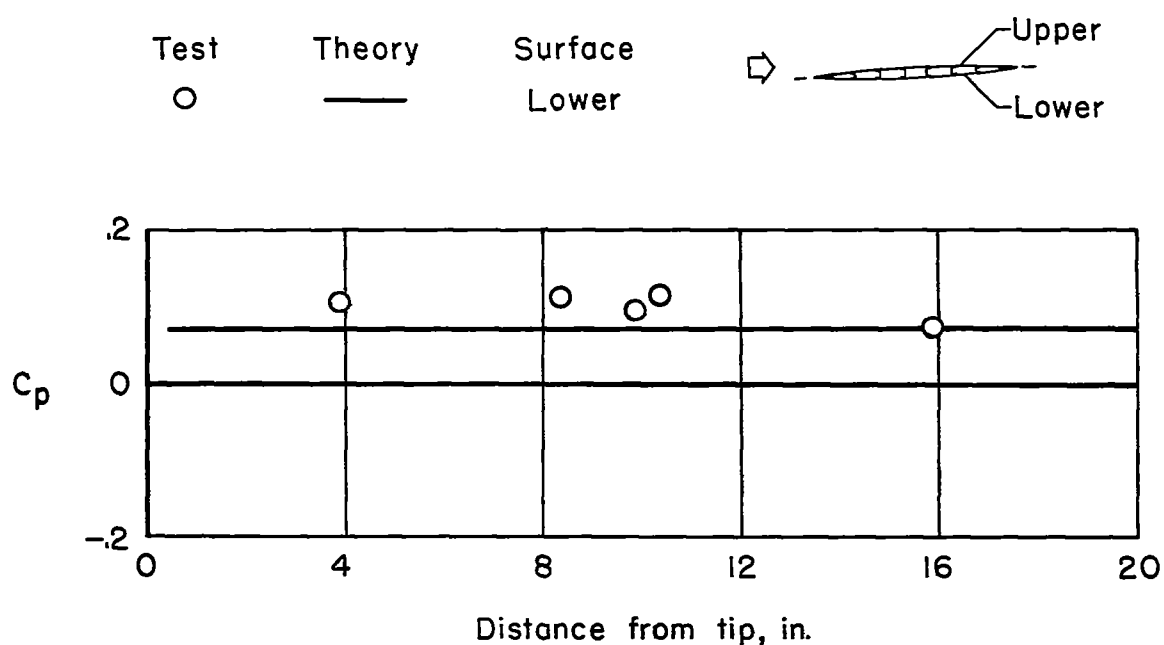
(a)   5/8 inch from leading edge.
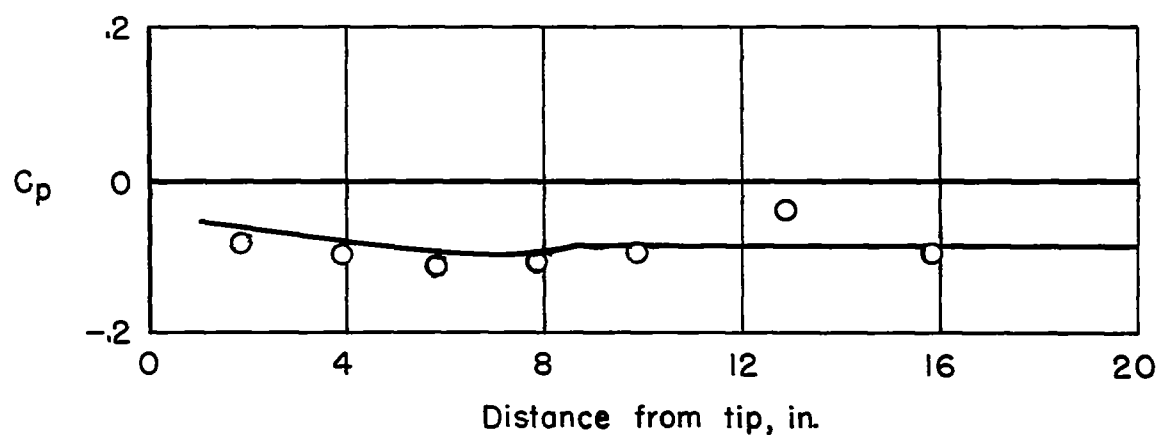
(b)   15 inches from leading edge.

Figure 14.- Spanwise pressure-coefficient distributions on model
MW-2-(3) at an angle of attack of -2°.
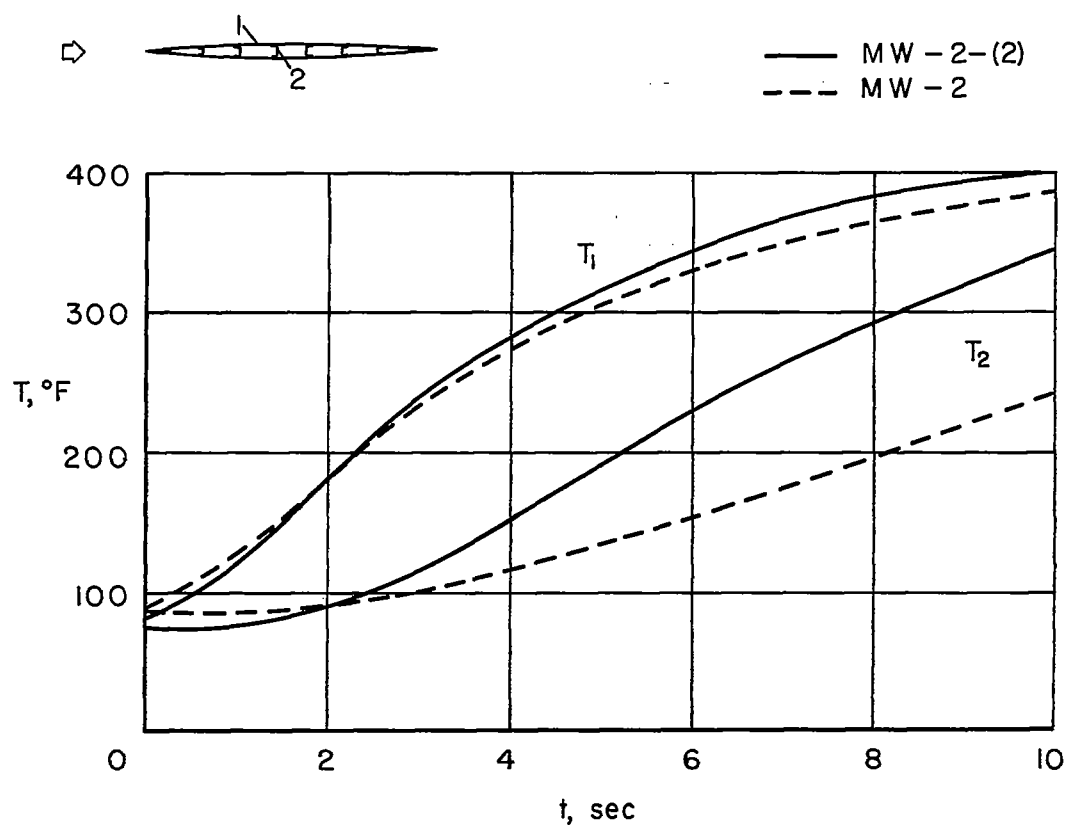
(a) Skin and web temperatures.
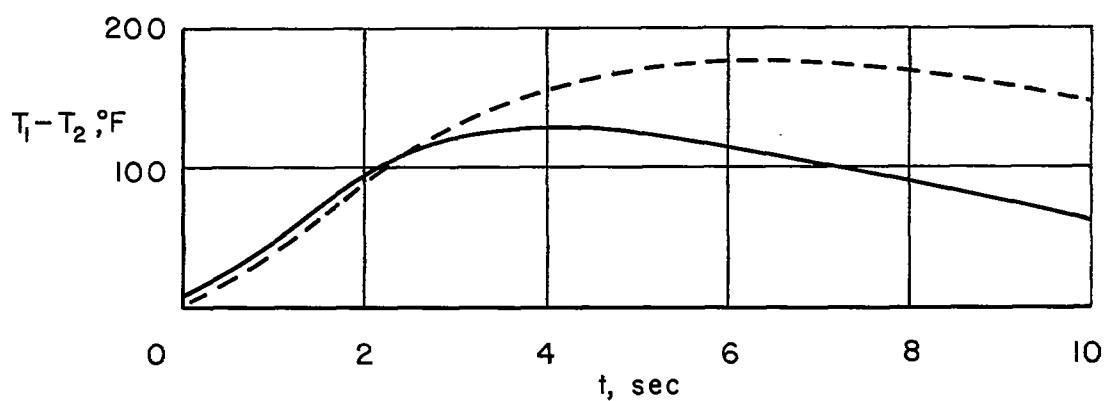
(b) Temperature differences.

Figure 15.- Comparison of maximum skin and minimum web temperatures and temperature differences in one skin and web combination.
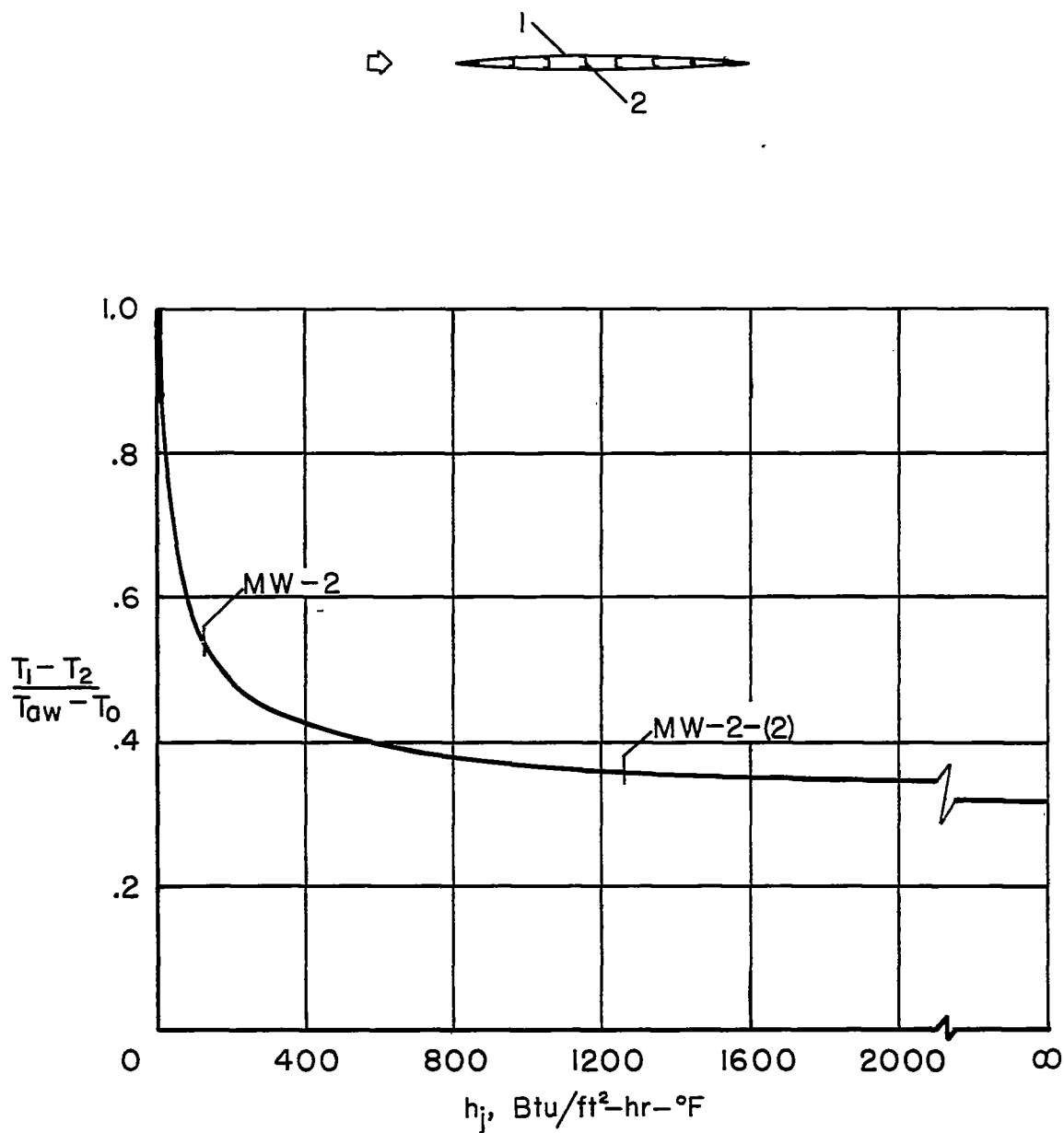
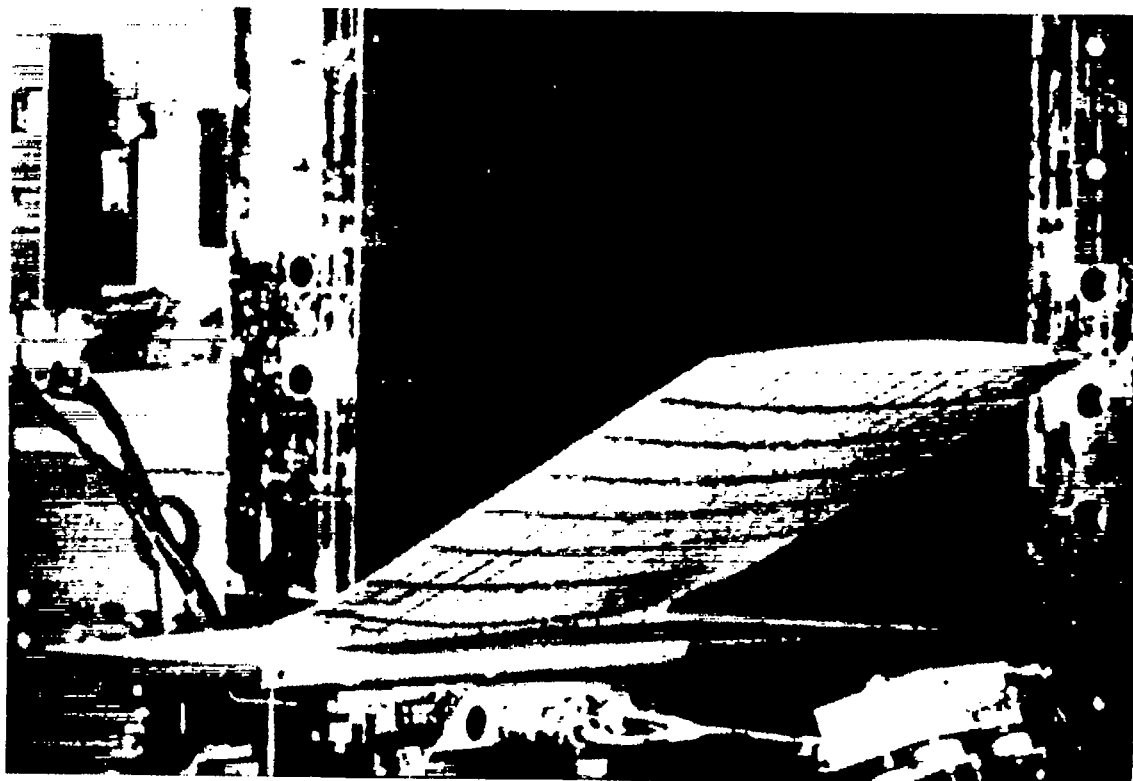Figure 16.- Variation with joint conductivity of maximum temperature difference in a skin and web combination.

Figure 17.- Model MW-2-(2) after failure.   L-57-2732